Theoretical Lifetime Extraction and Experimental Demonstration of Stable Cesium-Containing Tri-Cation Perovskite Solar Cells with High Efficiency

Rui Zhang[a], Detao Liu[a], Yafei Wang[a], Ting Zhang[a], Xiangling Gu[a], Peng Zhang[a], Jiang Wu[b], Zhi David Chen[a,c,*], Yingchun Zhao[d], Shibin Li[a,*]

[a] School of Optoelectronic Information, State Key Laboratory of Electronic Thin Films and Integrated Devices, University of Electronic Science and Technology of China (UESTC), Chengdu, 610054, China

[b] Department of Electronic and Electrical Engineering, University College London, Torrington Place, London WC1E 7JE, United Kingdom

[c] Department of Electrical & Computer Engineering and Center for Nanoscale Science & Engineering, University of Kentucky, Lexington, Kentucky 40506, USA

[d] Beijing Haidian District Vocational School, 100084, Beijing, China.

*Corresponding authors: shibinli@uestc.edu.cn, zhichen@engr.uky.edu

ABSTRACT

Despite the high power conversion efficiency, the severe performance degradation of organic-inorganic lead halide perovskite solar cells caused by moisture and thermal phase transition is an obstacle to commercialization of the perovskite solar cells. We propose the theoretical lifetime extraction of perovskite solar cells with a mixed-cations lead halide perovskite absorber containing $CH_3NH_3^+$, $CH_3(NH_2)_2^+$ and Cs^+. The estimated mean time to failure (MTTF) of the triple cation perovskite solar cells is up to 180 days in ambient. Compared with the perovskite solar cells based on $CH_3NH_3PbI_3$, the triple-cation perovskite solar cells, whose power conversion efficiency reaches 18.2% in this study, have a much better performance in terms of thermal stability and humidity stability. Improvements of both performance and stability pave the way for commercialization of perovskite solar cells.

Keywords:

triple-cation; perovskite solar cells; humidity stability; thermal stability; reliability

1. Introduction

The increasing energy demand and environmental concerns have led to renewed interest in recent years because of the rapid development of economy and industry. Solar energy is one of the most promising alternatives to fossil fuels because it is an abundant, clean, cheap and renewable energy source [1-7]. Among various types of photovoltaic devices, organic-inorganic lead halide perovskite solar cells have attracted much attention because of their excellent photo-voltaic performance and low cost in fabrication [8-14]. The power conversion efficiency (PCE) of perovskite solar cells (PSCs) has increased from 3.8% [15] to the current world record of 21.1% [16] from 2009 to 2016. Apart from PCE, stability is another important technical figure-of-merit of PSCs. In recent years, research reports keep delivering new record PCE of PSCs, but research about stability is lagging behind. The stability problem has become a bottleneck restricting the development of PSCs. If the instability matters can't be settled, the goal for high reproducibility and low cost won't be reached easily.

The archetypal compound for PSCs is methylammonium (MA) lead triiodide $CH_3NH_3PbI_3$ ($MAPbI_3$) [17-19]. But MA degrades easily when contacting with moisture and oxygen or at 55 °C [20-22]. By using black polymorph formamidinium (FA) lead triiodide $CH_3(NH_2)_2PbI_3$ ($FAPbI_3$) in mesoscopic structure, the PCE of PSCs achieved 16.01% [23]. However, pure $FAPbI_3$ is not stable even at room temperature as it can crystallize into two phases: one is hexagonal δ-phase (yellow color), and another is trigonal α-phase (black color) [24], which is sensitive to solvents or humidity [25]. Recently what caught the scientists' eyes in mixed cation

perovskites is the inorganic cesium (Cs) [26]. Park and co-workers demonstrated that a partial substitution of FA^+ by Cs^+ in $FAPbI_3$ perovskite can substantially enhance thermal and moisture stability [27], as shown in Table 1. Yi *et al.* showed that Cs is effective in "pushing" FA into the beneficial black perovskite phase due to entropic stabilization [28]. Grätzel and co-workers demonstrated a stabilized PCE over 18% up to 250 hours by using multiple A-cation formulations with incorporating Cs into FA/MA perovskites, but the specific improvement on stability was not described in detail [16].

Reliability evaluation based on degradation models is widely applied in highly reliable products as a cost effective way of evaluating their reliability [29]. By employing reliability analysis method, we can further analyze the mean time to failure, thus estimating the lifetime of the products [30]. This method is currently widely used in many industrial areas, used to estimate the product lifetime. And it is also widely used in scientific research. Vázquez and co-workers [31] tried to establish a frame of reference for the reliability of III-V concentrator cells, and they demonstrated that it is possible to achieve III-V high-concentration solar cells with operational lifetimes of more than 100000 h. Han *et al.* [32] established a large Dye-sensitized solar cell module, and the 85 °C life of the module was more than 500 h.

The mixed-cations Pb halide perovskite containing cesium has been reported in papers. And many articles also discuss the stability of the devices. However, a very limited study has been reported on detailed reliability analysis for PSCs. Previous studies of triple cation PSCs were devoted to improving the PCE or stability testing

[33,34] rather than reliability analysis and simulation of MTTF for PSCs. In this paper, for the first time, detailed reliability analysis of PSCs is presented. And we further estimated the value of MTTF by simulation. Here, both humidity and thermal stability are systematically investigated for triple cation perovskite solar cells. For comparison, two different types of solar cells have been prepared: one is the single MA cation PSCs based on $MAPbI_3$, and the other is triple cation solar cells with a mixture of a triple Cs/MA/FA cation and Br/I halide. The mean time to failure (MTTF) of the triple cation perovskite solar cells is estimated over 180 days in ambient, representing an 8-fold enhancement in stability over conventional MA cation PSCs. The maximum PCE of the triple cation PSCs and MA cation PSCs are 18.2% and 16.2%, respectively. The triple cation PSCs can be very stable in harsh environment of high-moisture (25-35%) and elevated temperature (>100 °C).

2. Experimental

FTO glasses were cleaned in the ultrasonic bath followed by drying with a N_2 flow. Then, a TiO_2 compact layer (c-TiO_2) was deposited on FTO by spray pyrolysis at 500 °C. A mesoporous TiO_2 (m-TiO_2) layer was deposited by spin coating. After going through a series of sintering steps, Li-doping of m-TiO_2 is accomplished by spin coating a 0.1 M solution of Li-TFSI in acetonitrile. To preparation two kinds of PSCs, MA cation perovskite solution or MA/FA/Cs cation perovskite solution was prepared respectively. The completely dissolved solution was spin-coated on the m-TiO_2 layer. Then the film was heated at heating platform in order to obtain a dense perovskite film. After the perovskite was annealed, the substrates were cooled down

for a few minutes. Then the spiro-OMeTAD solution was spin-coated at 4000 rpm for 30 s to get the hole transport layer (HTL). Finally, an ~80 nm of gold top electrode was deposited using thermal evaporation on the HTL. Detailed fabrication steps are presented in the Experimental section of the Supplementary Material.

3. Results and discussion

The stability problem of PSCs is caused by the chemical changes of the perovskite materials under certain environmental conditions. Different environmental conditions lead to different chemical stability problems. To address such environmental instabilities, triple cation PSCs are presented as follows.

Like conventional MA cation PSCs, the triple cation PSCs consist of a cathode, an electron transport layer (ETL), a perovskite light absorption layer, a hole transport layer (HTL), and an anode [35], as shown in Figure 1(a). The energy diagram of PSCs are shown in the Figure 1(b). A TiO_2 compact layer is used to transfer electrons generated in the conduction band of perovskite to the FTO conductive glass [36]. The TiO_2 compact layer not only transports electrons, but also acts as a barrier layer against the injection of holes, which suppresses the recombination of electron-hole pairs at the interface of FTO conductive substrate and improves the PCE of the solar cells [37]. At the same time, an HTL(sprio-OMeTAD) hole transport layer is used to achieve electron-hole pair separation. In Figure 1(c) and 1(d), we show the cross-sectional SEM images. The solar cell architecture is a stack of glass/FTO/compact TiO_2/Li- doped mesoporous TiO_2/perovskite/spiro-OMeTAD/gold.

The environmental conditions such as water and oxygen can directly influence

the stability of relevant components of perovskite materials, either during the material preparation or device operation. For example, as shown in the eq 1-3, $MAPbI_3$ is very sensitive to water [38].

$$CH_3NH_3PbI_3(s) \xleftrightarrow{H_2O} PbI_2(s) + CH_3NH_3I(aq) \quad (1)$$

$$CH_3NH_3I(aq) \leftrightarrow CH_3NH_2(aq) + HI(aq) \quad (2)$$

$$4HI(aq) + O_2(g) \rightarrow 2I_2(s) + H_2O(l) \quad (3)$$

There always exists a reaction of eq 1 if the $CH_3NH_3PbI_3$ film contacts with humid air. When there is CH_3NH_3I in the perovskite film, a reaction of eq 2 always exists. When reacting with oxygen, HI is decomposed into I_2 and H_2O. The reduction of HI can facilitate the reaction of eq 2 towards the right, resulting in further decomposition of CH_3NH_3I. As a result, it will further facilitate decomposition of $CH_3NH_3PbI_3$ as in eq 1. How to suppress or eliminate these reactions is the key for achieving stabled PSCs.

$FAPbI_3$ has a bandgap of 1.48 eV, which is smaller than that of $MAPbI_3$ [25]. This reduced bandgap may result in a broader absorption spectrum. In addition, $FAPbI_3$ has better thermal stability than $MAPbI_3$ due to the stronger internal interactions [39]. However, pure $FAPbI_3$ is not stable because the black perovskite α-phase was observed to turn into yellow $FAPbI_3$ δ-phase in an ambient humid atmosphere even at room temperature [24]. The incorporation of $MAPbBr_3$ into $FAPbI_3$ can stabilize the perovskite phase of $FAPbI_3$ [25]. But the formation of film dependent on processing conditions in the glove box closely. Meanwhile, the incorporation of MA may affect the thermal stability. The addition of Cs can not only inhibit the formation of yellow

phase in MA / FA perovskite, but also contribute to the temperature stability and reduce the environmental requirements of the film formation [16].

According to previous work, the ionic radius of MA^+, FA^+, Cs^+, Pb^{2+}, I^-, and Br^- are 2.17, 2.53, 1.67, 1.19, 2.20, and 1.96 Å, respectively [40,41]. Partial replacement of MA cation with slightly larger FA cation can increase the PCE of PSCs, but the stability of the devices will be reduced (Figure S4(b)). Goldschmidt tolerance factor (*t*) can predict stable crystal structures of perovskite materials, which can be calculated from the ionic radius of the atoms [42]. Non-perovskite structure is formed when the tolerance factor is higher than 1 or lower than 0.71. In the ABX_3 structure, if the size of A-ion decreases, or the size of B-ion increases, the *t* decreases [43]. A *t* value between 0.8 and 1.0 is favorable for a stable perovskite structure [44]. Cs^+ is smaller than FA^+ or MA^+. The incorporation of Cs^+ leads to the reducing of effective cation radius of triple-cation perovskite compound. The combination of Cs^+, FA^+ and MA^+ can adjust *t* to the range in which the cubic lattice structure that matches the stable perovskite phase can be formed. Cs^+ can be thought of as a “stabilizer” of the perovskite phase [42]. It can stabilize the photoactive black phase and suppress the transition of the hexagonal yellow phase of FA perovskite, which is in agreement with the reports of Lee e*t al.* [27] Yi *et al.* demonstrated that the incorporation of Cs in PSCs can exhibit negligible hysteresis and excellent long term stability in ambient air [28]. They illustrated this remarkable behavior with the first principle computations and showed that the perovskite phase is significantly stabilized by mixing the A-cations stems from entropic gains and the small internal energy input required for

the formation of their solid solution. And Li e*t al.* also observed that if the concentration of Cs is too high, the phase separation will be caused due to the large gap between the ion radius [42]. The mixture of the three kinds of cation can avoid this phenomenon. So the stability of the triple cation perovskite materials can be increased.

In order to compare the overall performance of the devices based on the two kinds of materials, we have fabricated solar cells based on each type of perovskites (see Supplementary Material). It is observed that the devices based on three cations achieved an average PCE of 16.84% and a maximum PCE of 18.2%, which is significantly improved compared to the MA cation devices with an average PCE of only 14.0%, and a maximum PCE of 16.2%. Figure 2(a) shows the J-V curves of the best-performed PSCs based on triple cation perovskite and MA cation perovskite. All device parameters and the standard deviation are listed in Table 2. The average open circuit voltage (V_{OC}), fill factor (FF), and short circuit current density (J_{SC}) of triple cation PSCs are 1.09 V, 22.98mA/cm^2, and 67.1%, respectively. The average V_{OC}, FF and J_{SC} of the MA cation PSCs are 1.01 V, 21.50mA/cm^2, and 64.4%, respectively. The higher J_{SC} of triple cation perovskite film is related to the higher light absorption.

In Figure 2(b), we depict the UV-visible absorption spectra of the two types of perovskite films. As is seen from the figure, the absorption intensity of the triple cation perovskite film is higher than that of the MA cation perovskite film. This may be related to a higher thickness of the triple cation perovskite film which can be seen in the Figure 1(c) and 1(d). It is worth noting that the thicknesses of the two films

have already been optimized to obtain the optimum device performance.

To discern the charge transport characteristics of PSCs, electrochemical impedance spectroscopy (EIS) analysis was conducted. Figure 2(c) shows the Nyquist curves of MA cation and Cs/FA/MA cation devices under 1 sun illumination. A suitable equivalent electronic circuit model [45] (the inset of figure 2(c)) was used to fit the EIS data. Two arcs were obtained in the Nyquist plots, where the first arc in the high frequency range is related to the transport and extraction in the cathode and the second arc is related to recombination resistance. Obviously, the Nyquist plots show that transport resistance of triple cation devices is smaller than MA cation devices. A smaller transport resistance in the triple cation device confirms the superior charge transport property, and it also consistent with the smaller series resistance (Rs) value from the light J-V curve.

Besides a high PCE, another major concern is whether PSCs are durable in practical applications. We investigated solar cells under constant humidity of 25%-35% in dark condition (T=25 °C) without encapsulation (the devices were exposed directly to the ambient environment, without any cover). To ensure the result accuracy, eight devices were tested for each kind of samples. As is seen in Figure 3(a), devices employing Cs/FA/MA cations show clearly better stability than the pristine $MAPbI_3$ based devices. In terms of PCE of the Cs/FA/MA based devices, the performance of the majority devices was retained for 15 days and shows marginal 1% degradation after 4 days. Whereas the pristine $MAPbI_3$ devices degraded dramatically, its PEC degraded by 10% after 4 days and 30% after 15 days. The key photo-voltaic

parameters including V_{OC}, FF, J_{SC} and PCE of devices before and after the aging test in dark condition after 15 days are summarized in Figure S1(a)-(d). And we further tested the stability of the device under high humidity conditions (humidity=60~80 %) [33]. Triple cation perovskite devices still show better stability than MA cation perovskite devices at high humidity environments, as shown in figure 3(c). Enhanced stability of triple cation perovskite solar cells in ambient condition is attributed to better material stability against humidity. The δ phases of $FAPbI_3$ and $CsPbI_3$ differ significantly in their atomic structure and the volume per stoichiometric unit, but the α and β phase are very similar to the two systems [28]. For the perovskite phases, either the α and β types, the sum of the energetic and mixing entropy contributions to the free energy is favorable, resulting in a stabilization of the mixed phases. The δ→α or β transition temperature is reduced by ~200-300 K when going from the pure $FAPbI_3$ to the mixed $Cs_xFA1_xPbI_3$ system.

Reliability is the ability of a system or device to perform work under certain conditions within a certain amount of time [46]. So the reliability can be evaluated by defining the function of the system or device. For PSCs, the function can be set to photoelectric power conversion. The normalized conversion efficiency we set is relative to the initial efficiency. If the cell efficiency is greater than the prefined value(P_{limit}, here it can be set to 70% of the initial efficiency) in a given time t, it is considered to be operational, otherwise it is considered to be failed. The PCE of the solar cells is normalized to its initial value.

For a large number of devices, efficiency is subject to normal distribution. The

power probability density function can be written as:

$$p(P,t)=\frac{1}{\sqrt{2\pi}\sigma(t)}\exp\left[-\frac{1}{2}\left(\frac{P(t)-\mu(t)}{\sigma(t)}\right)^2\right] \quad (4)$$

Where P(t) is the PCE of PSCs, μ(t) is its average value and σ(t) is standard deviation [29]. Both μ(t) and σ(t) can be obtained experimentally. The average PCE, μ(t), generally decreases exponentially, and thus can be described as

$$\mu(t)=A\exp(-\alpha t)+y_0 \quad (5)$$

The parameters in the equation were fitted by the nonlinear least squares method, as shown in Table 3. The experimental points and the fitting curve are shown in Figure 4. The standard deviation σ(t) increases linearly with time, and it would be described as

$$\sigma(t)=\sigma_0+Bt \quad (6)$$

σ_0=0 because σ_0 is the standard deviation of the μ(t) at t= 0. The parameter B was fitted by the least squares method, as shown in Table 3. The experimental points and the fitting curve are shown in Figure 4.

The reliability R(t) is a function of time. The reliability can give a probability that the PCE of the device in all the number of PSCs is higher than the predetermined PCE (P_{limit}) after a certain period of time. So R(t) can be calculated by the power probability density function, as follows:

$$R(t)=\int_{P_{limit}}^{\infty}p(P,t)dP=1-\Phi\left(\frac{P_{limit}-\mu(t)}{\sigma(t)}\right) \quad (7)$$

where Φ is the cumulative probability function for the Gaussian distribution [46].

The accumulated operation time extrapolated at room temperature and the cell failures can be statistically described by the Weibull distribution. At a given time, if

PCE is lower than P_{limit}, the solar cell is considered to be failed. In this test, failure of a single solar cell was defined as a power loss of 30% or more with respect to the initial value. In this case the reliability as a function of time is expressed by eq 8, where β is the shape parameter and η is the scale factor of the Weibull distribution. The reliability data is obtained by using the method above. In this study, β and η are obtained by the fitting the failure probability curves. From the values of β and η, the MTTF can be estimated with eq 9, where Γ is Euler's Gamma function [47], as shown in Table 4. There is a big difference in the calculated value of the MTTF for PSCs based on triple cation and that based on MA cation. The MTTF is 4425.8 h for PSCs based on triple cation and 516 h for that based on MA cation, thus demonstrating a >8-fold enhancement of the cell lifetime. If P_{limit} is $0.8P_0$ or $0.9P_0$, the MTTF is 1704.9 h and 293.3 h respectively for PSCs based on triple cation, and it is only 238.1 h and 93.6 h for PSCs based on MA cation, as shown in Table 4. In Figure 3(b) the plot of the reliability functions of PSCs as a function of aging time is presented, taking into account the Weibull parameters of Table 4. The MTTF and the corresponding parameters of the devices in high humidity environment are shown in Table 5.

$$R(t) = \exp\left[-\left(\frac{t}{\eta}\right)^{\beta}\right] \quad (8)$$

$$MTTF = \eta\Gamma\left(1+\frac{1}{\beta}\right) \quad (9)$$

In the application of solar cells, the temperature of device will rise under the light conditions. Therefore, we need to detect the PCE stability of the device under heating

conditions. According to other group's study, 56 °C is the transition temperature of $MAPbI_3$ from tetragonal to cubic crystal [48]. In general, the standard temperature for thermal stability testing of commercial applications for solar cells is 85 °C [49]. We tested the normalized PCE changes of two different kinds of devices under heating conditions at 85 °C as a function of time, as shown in Figure 3(e). After a period of time, the color of devices based on MA cation perovskite began to change from the dark brown to yellow. This change in color is related to the generation of PbI_2 which is related to the decomposition of $MAPbI_3$ [50]. As shown in the figure, the PCE of the device based on MA cation has decreased dramatically to 20% of the original PCE after heating at 85 °C for 200 min, but the PCE of the device based on triple cation perovskite has maintained almost 80% of the original PCE. Similar to the reliability analysis for PSCs tested under high humidity, the MTTF of the PSCs tested at 85 °C is calculated and shown in Table 6. There is also a big difference in the most likely value of the MTTF for PSCs based on triple cation and that based on MA cation. The MTTF is 1682.7 min for PSCs based on triple cation and only 57.4 min for that based on MA cation, when $P_{limit}=0.7P_0$. The MTTF is also listed in the Table 6 if P_{limit} is $0.8P_0$ or $0.9P_0$. The estimated reliability functions are shown in Figure 3(f), which use the Weibull parameters listed in Table 6. Experiments show that the triple cation perovskite materials do promote thermal stability of the solar cells and a 30-fold enhancement($P_{limit}=0.7P_0$) in MTTF is estimated for cesium-containing tri-cation perovskite solar cells operating at elevated temperatures.

In order to further analyze the oxygen and moisture stability, we show X-ray

diffraction (XRD) patterns of the two types of perovskite films in Figure 6(a). All as-prepared films exhibit an obvious perovskite peak at 14.2° in the XRD patterns of both MA cation perovskite film and triple cation perovskite film. However, in the XRD patterns of the samples placed under constant humidity of 25%-35% in dark condition (T=25 °C) for 4 days, we can clearly note a new diffraction peak at 12.7° for MA cation perovskite film, corresponding to the (001) diffraction peak of cubic PbI_2 which is often observed as the final product from degraded lead iodide based perovskites [51]. There is no obvious change in the triple cation perovskite film, suggesting the addition of FA and Cs increases the moisture stability of the perovskite material [52,53]. In order to further analyze the temperature stability, we heat the two types of perovskite films at 130 °C for 3 hours. The XRD patterns of perovskite films before and after the thermal treatment are shown in Figure 6(b). This heating process results in rapid degradation of $MAPbI_3$, which was characterized by a change in color from dark brown to yellow. We can clearly find that the MA cation perovskite material decomposed and generated PbI_2 after heating for 3 hours, leading to a distinct change in perovskite diffraction peak. However, the color of triple cation materials did not obviously change after heating for 3 hours and the peak value of perovskite diffraction did not change much for the same heating time.

After storing the materials in dark environment with constant humidity of 25%-35% and constant temperature (T=25 °C) for 20 days, we can clearly find that the absorption of the two materials in the UV-visible range is very different (Figure 6(c) and 6(d)). The difference locates mainly in the range of 550-750 nm. In Figure

S3(a), we depict the normalized absorption variation with time at 630 nm. Due to the decomposition of $CH_3NH_3PbI_3$, the absorption in the UV-visible range is reduced. The triple cation perovskite film shows excellent humidity stability, and no obvious absorption change can be observed. We characterize the thermal stability of the two types of materials further by assessing their absorption. In Figure 6(e) and 6(f), we depict the UV-visible absorption spectra of MA cation perovskite and triple cation perovskite films before and after being kept at 130 °C for 300 min in dry air. It is evident that the perovskite film based on MA cation begins to bleach after the aggressive thermal stress test, which is confirmed by the reduced absorption spectroscopy. On the other hand, triple cation perovskite film remains dark black and does not bleach obviously. The absorption baseline of both two kinds of films in the wavelength range above 800 nm in the absorption spectrums are obviously increased because of the enhanced scattering effect induced by the rougher surface of the films after heating at high temperature. Although some degradation is visible, it is not as significant as the MA cation film. Figure S3(b) shows normalized absorption changes at 630 nm as a function of time. As shown in the Figure S3(b), there is more severe degradation at 630nm (16%) for MA cation than degradation of triple cation perovskite (4%) after heating for 300 min. The poor temperature stability of $MAPbI_3$ is due to accelerated dissociation of MA cation perovskite. The triple cation perovskite is expected to be more stable because the incorporation of Cs can prevent the phase transition of perovskite and also suppress the decomposition of $MAPbI_3$ as evidenced by XRD in Figure 6(b).

4. Conclusion

In summary, highly efficient triple cation PSCs were successfully fabricated by the combinations of three kinds of cations ($CH_3NH_3^+$, $CH_3(NH_2)_2^+$, Cs^+). By using MTTF method, we systematically investigated the reliability of both the triple cation PSCs and MA cation PSCs under constant humidity and high temperature condition. Detailed reliability analysis revealed that significant lifetime enhancement can be achieved for cesium-containing tri-cation perovskite solar cells operating at both high humidity and high temperature conditions. In addition, the maximum PCE of triple cation PSCs is achieved 18.2%, and that of devices based on MA cation is only 16.2%. The average efficiency of triple cation PSCs reached 16.84%, and that of devices based on MA cation is only 14.0%.

Acknowledgements

This work was supported by National Natural Science Foundation of China under Grant Nos. 61421002, 61574029, and 61371046. This work was also partially supported by University of Kentucky.

References

[1] S. Li, P. Zhang, H. Chen, Y. Wang, D. Liu, J. Wu, H. Sarvari, Z.D. Chen, Mesoporous PbI_2 assisted growth of large perovskite grains for efficient perovskite solar cells based on ZnO nanorods, J. Power Sources 342 (2017) 990-997.

[2] B. Cai, Y. Xing, Z. Yang, W.H. Zhang, J. Qiu, High performance hybrid solar cells sensitized by organolead halide perovskites, Energy Environ. Sci. 6 (2013) 1480-1485.

[3] Y. Yu, C. Wang, C.R. Grice, N. Shrestha, J. Chen, D. Zhao, W. Liao, A.J. Cimaroli, P.J. Roland, R.J. Ellingson, Y. Yan, Improving the Performance of Formamidinium and Cesium Lead Triiodide Perovskite Solar Cells using Lead Thiocyanate Additives, ChemSusChem 9 (2016) 3288-3297.

[4] S.C. Chen, N.Z. She, K.H. Wu, Y.Z. Chen, W.S. Lin, J.X. Li, F.I. Lai, J.Y. Juang, C.W. Luo, L.T. Cheng, T.P. Hsieh, H.C. Kuo, Y.L. Chueh, Crystalline Engineering Toward Large-Scale High-Efficiency Printable Cu(In,Ga)Se_2 Thin Film Solar Cells on Flexible Substrate by Femtosecond Laser Annealing Process, ACS Appl. Mater. Inter. 9(2017) 14006-14012.

[5] S. Li, P. Zhang, Y. Wang, H. Sarvari, D. Liu, J. Wu, Y. Yang, Z. Wang, Z.D. Chen, Interface engineering of high efficiency perovskite solar cells based on ZnO nanorods using atomic layer deposition, Nano Research 10 (2017) 1092-1103.

[6] Y. Zheng, T. Goh, P. Fan, W. Shi, J. Yu, A.D. Taylor, Toward Efficient Thick Active PTB7 Photovoltaic Layers Using Diphenyl Ether as a Solvent Additive, ACS Appl. Mater. Inter. 8 (2016) 15724-15731.

[7] S. Xing, H. Wang, Y. Zheng, J. Yu, Förster resonance energy transfer and energy cascade with a favorable small molecule in ternary polymer solar cells, Solar Energy 139 (2016) 221-227.

[8] P. Gao, M. Grätzel, M.K. Nazeeruddin, Organohalide lead perovskites for photovoltaic applications, Energy Environ. Sci. 7 (2014) 2448-2463.

[9] D. Liu, S. Li, P. Zhang, Y. Wang, R. Zhang, H. Sarvari, F. Wang, J. Wu, Z. Wang, Z.D. Chen, Efficient planar heterojunction perovskite solar cells with Li-doped compact TiO_2 layer, Nano Energy 31 (2017) 462-468.

[10] D. Zhao, Y. Yu, C. Wang, W. Liao, N. Shrestha, C.R. Grice, A.J. Cimaroli, L. Guan, R.J. Ellingson, K. Zhu, X. Zhao, R.G. Xiong, Y. Yan, Low-bandgap mixed

tin‐lead iodide perovskite absorbers with long carrier lifetimes for all-perovskite tandem solar cells, Nature Energy 2(2017) 17018.

[11] G. Hodes, Perovskite-Based Solar Cells, Science 342 (2013) 317-318.

[12] P. Gao, K.T. Cho, A. Abate, G. Grancini, P.Y. Reddy, M. Srivasu, M. Adachi, A. Suzuki, K. Tsuchimoto, M. Grätzel, M.K. Nazeeruddin, An efficient perovskite solar cell with symmetrical Zn (II) phthalocyanine infiltrated buffering porous Al_2O_3 as the hybrid interfacial hole-transporting layer, Phys. Chem. Chem. Phys. 18(2016) 27083-27089.

[13] D. Zheng, G. Yang, Y. Zheng, P. Fan, R. Ji, J. Huang, W. Zhang, J. Yu, Carbon Nano-Onions as a Functional Dopant to Modify Hole Transporting Layers for Improving Stability and Performance of Planar Perovskite Solar Cells, Electrochimica Acta. 247 (2017) 548-557.

[14] Y. Wang, S. Li , P. Zhang, D. Liu, X. Gu, H. Sarvari, Z. Ye, J. Wu, Z. Wang, Z.D. Chen. Solvent annealing of PbI_2 for the high-quality crystallization of perovskite films for solar cells with efficiencies exceeding 18%, Nanoscale 8 (2016) 19654-19661.

[15] A. Kojima, K. Teshima, Y. Shirai, T. Miyasaka, Organometal Halide Perovskites as Visible-Light Sensitizers for Photovoltaic Cells, J. Am. Chem. Soc. 131 (2009) 6050-6051.

[16] M. Saliba, T. Matsui, J.Y. Seo, K. Domanski, J.P. Correa-Baena, M.K. Nazeeruddin, S.M. Zakeeruddin, W. Tress, A. Abate, A. Hagfeldt, M. Grätzel, Cesium-containing triple cation perovskite solar cells: improved stability, reproducibility and high efficiency, Energy Environ. Sci. 9 (2016) 1989-1997.

[17] H.S. Jung, N.G. Park, Perovskite Solar Cells: From Materials to Devices, Small 11 (2015) 10-25.

[18] M. Wang, S. Li, P. Zhang, Y. Wang, H. Li, Z. Chen, A modified sequential method used to prepare high quality perovskite on ZnO nanorods, Chem. Phys. Lett. 639 (2015) 283-288.

[19] H. Li, S. Li, Y. Wang, H. Sarvari, P. Zhang, M. Wang, Z. Chen, A modified sequential deposition method for fabrication of perovskite solar cells, Solar Energy 126 (2016) 243-251.

[20] C.C. Stoumpos, C.D. Malliakas, M.G. Kanatzidis, Semiconducting Tin and Lead Iodide Perovskites with Organic Cations: Phase Transitions, High Mobilities, and Near-Infrared Photoluminescent Properties, Inorg. Chem. 52 (2013) 9019-9038.

[21] J.H. Noh, S.H. Im, J.H. Heo, T.N. Mandal, S.I. Seok, Chemical Management for Colorful, Efficient, and Stable Inorganic-Organic Hybrid Nanostructured Solar Cells, Nano Lett. 13 (2013) 1764-1769.

[22] G. Niu, W. Li, F. Meng, L. Wang, H. Dong, Y. Qiu, Study on the stability of $CH_3NH_3PbI_3$ films and the effect of post-modification by aluminum oxide in all-solid-state hybrid solar cells, J. Mater. Chem. A 2 (2014) 705-710.

[23] J.W. Lee, D.J. Seol, A.N. Cho, N.G. Park, High-Efficiency Perovskite Solar Cells Based on the Black Polymorph of $HC(NH_2)_2PbI_3$, Adv. Mater. 26 (2014) 4991-4998.

[24] G.E. Eperon, S.D. Stranks, C. Menelaou, M.B. Johnston, L.M. Herz, H.J. Snaith, Formamidinium lead trihalide: a broadly tunable perovskite for efficient planar heterojunction solar cells, Energy Environ. Sci. 7 (2014) 982-988.

[25] N.J. Jeon, J.H. Noh, W.S. Yang, Y.C. Kim, S. Ryu, J. Seo, S.I. Seok, Compositional engineering of perovskite materials for high-performance solar cells, Nature 517 (2015) 476-480.

[26] A. Amat, E. Mosconi, E. Ronca, C. Quarti, P. Umari, M.K. Nazeeruddin, M.

Grätzel, F.D. Angelis, Cation-Induced Band-Gap Tuning in Organohalide Perovskites: Interplay of Spin-Orbit Coupling and Octahedra Tilting, Nano Lett. 14 (2014) 3608-3616.

[27] J.W. Lee, D.H. Kim, H.S. Kim, S.W. Seo, S.M. Cho, N.G. Park, Formamidinium and Cesium Hybridization for Photo- and Moisture-Stable Perovskite Solar Cell, Adv. Energy Mater. 5 (2015) DOI: 10.1002/aenm.201501310.

[28] C. Yi, J. Luo, S. Meloni, A. Boziki, N. Ashari-Astani, C. Grätzel, S.M. Zakeeruddin, U. Röthlisberger, M. Grätzel, Entropic stabilization of mixed A-cation ABX_3 metal halide perovskites for high performance perovskite solar cells, Energy Environ. Sci. 9 (2016) 656-662.

[29] M. Vázquez, I. Rey-Stolle, Photovoltaic module reliability model based on field degradation studies, Prog. Photovol.: Res. Appl. 16 (2008) 419-433.

[30] J. Kim, N. Park, J.S. Yun, S. Huang, M.A. Green, A.W.Y. Ho-Baillie, An effective method of predicting perovskite solar cell lifetime-Case study on planar $CH_3NH_3PbI_3$ and $HC(NH_2)_2PbI_3$ perovskite solar cells and hole transfer materials of spiro-OMeTAD and PTAA, Sol. Energy Mater. Sol. Cells 162 (2017) 41-46.

[31] M. Vázquez, C. Algora, I. Rey-Stolle, J.R. González, III-V Concentrator Solar Cell Reliability Prediction Based on Quantitative LED Reliability Data, Prog. Photovolt.: Res. Appl. 15 (2007) 477-491.

[32] C. Han, S. Park, W. Oh, Reliability-based structural optimization of 300×300 mm(2) dye-sensitized solar cell module, Sol. Energy 150 (2017) 128-135.

[33] L. Zhang, X. Zhang, Y. Yu, X. Xu, J. Tang, X. He, J. Wu, Z. Lan, Efficient planar perovskite solar cells based on high-quality perovskite films with smooth surface and large crystal grains fabricated in ambient air conditions, Sol. Energy 155 (2017) 942-950.

[34] L. Zhang, X. Zhang, X. Xu, J. Tang, J. Wu, Z. Lan, CH_3NH_3Br Additive for Enhanced Photovoltaic Performance and Air Stability of Planar Perovskite Solar Cells prepared by Two-Step Dipping Method, Energy Technology 5 (2017) 1887-1894.

[35] Y. Zhao, X. Xu, H. Zhang, J. Shi, L. Zhu, H. Wu, D. Li, Y. Luo, Q. Meng, Sequential multi-drop coating method for large crystallized α-$(NH_2)_2CHPbI_3$ and mixed-organic-cation perovskite films for highly efficient mesoscopic perovskite solar cells, J. Power Sources 359 (2017) 147-156.

[36] Y. Yang, K. Ri, A. Mei, L. Liu, M. Hu, T. Liu, X. Li, H. Han, The size effect of TiO_2 nanoparticles on a printable mesoscopic perovskite solar cell, J. Mater. Chem. A 3 (2015) 9103-9107.

[37] X. Yin, Y. Guo, Z. Xue, P. Xu, M. He, B. Liu, Performance enhancement of perovskite-sensitized mesoscopic solar cells using Nb-doped TiO_2 compact layer, Nano Research 8 (2015) 1997-2003.

[38] J.M. Frost, K.T. Butler, F. Brivio, C.H. Hendon, M. Schilfgaarde, A. Walsh, Atomistic Origins of High-Performance in Hybrid Halide Perovskite Solar Cells, Nano Lett. 14 (2014) 2584-2590.

[39] Y. Liu, J. Sun, Z. Yang, D. Yang, X. Ren, H. Xu, Z. Yang, S. Liu, 20-mm-Large Single-Crystalline Formamidinium-Perovskite Wafer for Mass Production of Integrated Photodetectors, Odv. Opt. Mater. 4 (2016) 1829-1837.

[40] G.P. Nagabhushana, R. Shivaramaiah, A. Navrotsky, Direct calorimetric verification of thermodynamic instability of lead halide hybrid perovskites, Proc. Nat. Acad. Sci. 113 (2016) 7717-7721.

[41] W. Travis, E.N.K. Glover, H. Bronstein, D.O. Scanlon, R.G. Palgrave, On the application of the tolerance factor to inorganic and hybrid halide perovskites: a

revised system, Chem. Sci. 7 (2016) 4548-4556.

[42] Z. Li, M. Yang, J.S. Park, S.H. Wei, J.J. Berry, K. Zhu, Stabilizing Perovskite Structures by Tuning Tolerance Factor: Formation of Formamidinium and Cesium Lead Iodide Solid-State Alloys, Chem. Mater. 28 (2015) 284-292.

[43] J.P. Correa-Baena, A. Abate, M. Saliba, W. Tress, T.J. Jacobsson, M. Grätzel, A. Hagfeldt, The rapid evolution of highly efficient perovskite solar cells, Energy Environ. Sci. 10 (2017) 710-727.

[44] D.B. Mitzi, Synthesis, Structure, and Properties of Organic-Inorganic Perovskites and Related Materials, Progress Inorg. Chem. 48 (2007) 1-121.

[45] M.A. Mahmud, N.K. Elumalai, M.B. Upama, D. Wang, K.H. Chan, M. Wright, C. Xu, F. Haque, A. Uddin, Low temperature processed ZnO thin film as electron transport layer for efficient perovskite solar cells, Sol. Energy Mater. Sol. Cells 159 (2017) 251-264.

[46] J.R. González, M. Vázquez, C. Algora, N. Núñez, Real-time reliability test for a CPV module based on a power degradation model, Prog. Photovolt.: Res. Appl. 19 (2011) 113-122.

[47] J.R. González, M. Vázquez, N. Núñez, C. Algora, I. Rey-Stolle, B. Galiana, Reliability analysis of temperature step-stress tests on III-V high concentrator solar cells, Microelectronics Reliability 49 (2009) 673-680.

[48] T. Baikie, Y. Fang, J.M. Kadro, M. Schreyer, F. Wei, S.G. Mhaisalkar, M. Grätzel, T.J. White, Synthesis and crystal chemistry of the hybrid perovskite $(CH_3NH_3)PbI_3$ for solid-state sensitised solar cell applications, J. Mater. Chem. A 1 (2013) 5628-5641.

[49] Y. Fang, X. Wang, Q. Wang, J. Huang, T. Wu, Impact of annealing on spiro-OMeTAD and corresponding solid-state dye sensitized solar cells, Phys.

Status Solidi A 211 (2014) 2809-2816.

[50] A. Dualeh, P. Gao, S.I. Seok, M.K. Nazeeruddin, M. Grätzel, Thermal Behavior of Methylammonium Lead-Trihalide Perovskite Photovoltaic Light Harvesters, Chem. Mater. 26 (2014) 6160-6164.

[51] X. Dong, X. Fang, M. Lv, B. Lin, S. Zhang, J. Ding, N. Yuan, Improvement of the humidity stability of organic-inorganic perovskite solar cells using ultrathin Al_2O_3 layers prepared by atomic layer deposition, J. Mater. Chem. A 3 (2015) 5360-5367.

[52] D.P. McMeekin, G. Sadoughi, W. Rehman, G.E. Eperon, M. Saliba, M.T. Hörantner, A. Haghighirad, N. Sakai, L. Korte, B. Rech, M.B. Johnston, L.M. Herz, H.J. Snaith, A mixed-cation lead mixed-halide perovskite absorber for tandem solar cells, Science 351 (2016) 151-155.

[53] A. Binek, F.C. Hanusch, P. Docampo, T. Bein, Stabilization of the Trigonal High-Temperature Phase of Formamidinium Lead Iodide, J. Phys. Chem. Lett. 6 (2015) 1249-1253.

Figures and Tables

Fig. 1. (a) Schematic illustration of the device structure of mesoporous PSCs. (b) Energy band diagram of the PSCs. Cross-sectional SEM images of (c) MA-based PSCs and (d) the triple-cation (Cs/FA/MA) PSCs.

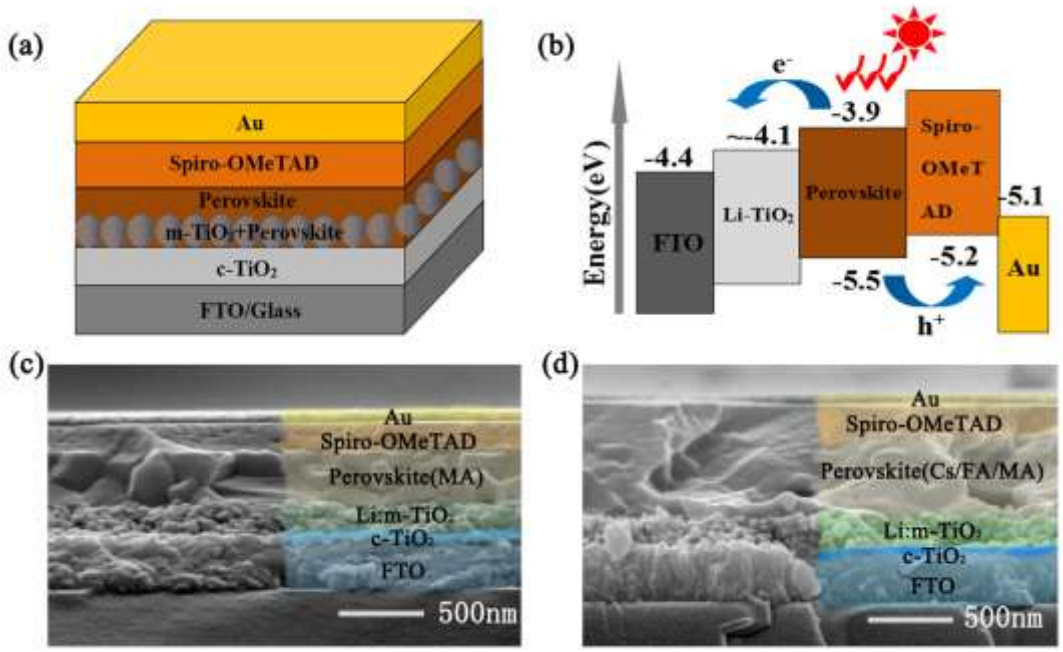

Fig. 2. (a) J-V curves of the best-performance PSCs based on MA cation perovskite and triple cation (Cs/FA/MA) perovskite. (b) Comparison of UV-visible absorption spectra of the two kinds of perovskite film. (c) Nyquist plot of the PSCs based on MA cation perovskite and triple cation (Cs/FA/MA) perovskite.

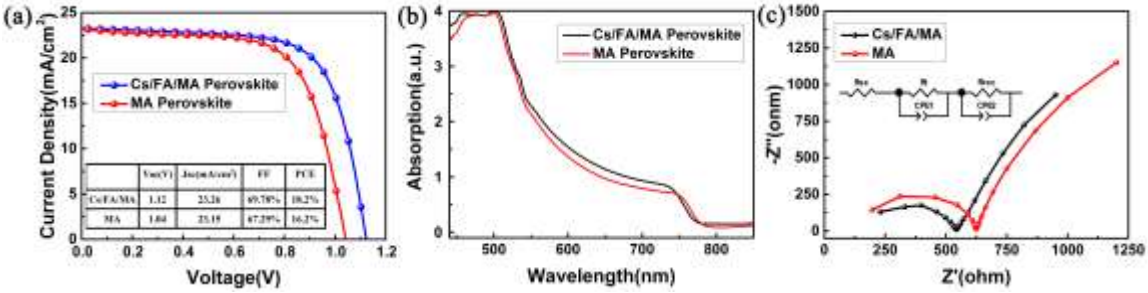

Fig. 3. (a) Normalized PCE of the PSCs treated in an ambient environment (humidity 25%- 35%, T=25 °C) , (c) in high humidity environment (humidity 60%- 80%, T=25 °C) and (e) annealed at 85 °C. (b) The estimated reliability functions at room temperature, (d) at high humidity and (f) at 85 °C.

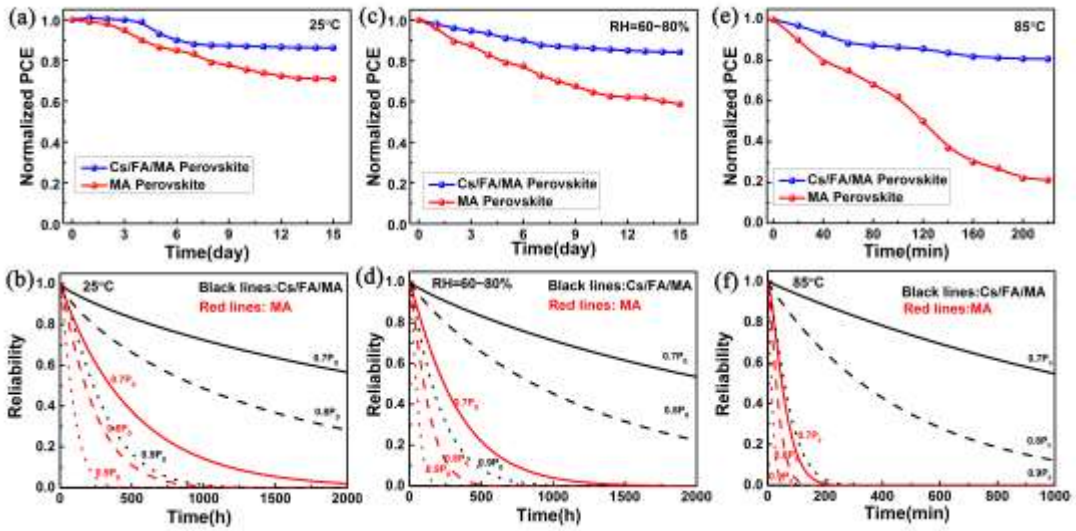

Fig. 4. The μ(t) of (a) triple cation PSCs and (b) MA cation PSCs at room temperature. The σ(t) of (c) triple cation PSCs and (d) MA cation PSCs at room temperature. The μ(t) of (e) triple cation PSCs and (f) MA cation PSCs at high humidity. The σ(t) of (g) triple cation PSCs and (h) MA cation PSCs at high humidity.The μ(t) of (i) triple cation PSCs and (j) MA cation PSCs at 85 °C. The σ(t) of (k) triple cation PSCs and (l) MA cation PSCs at 85 °C.

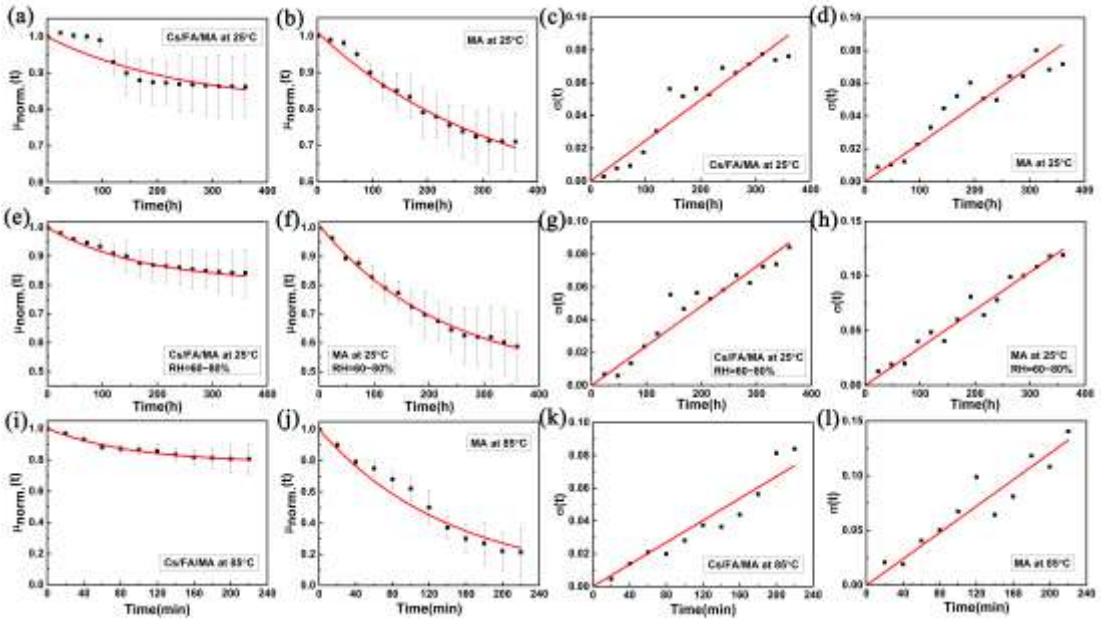

Fig. 5. Schemes of aging for the MA cation perovskite film and Cs/FA/MA cation perovskite film. The yellow spot in the scheme of the MA cation sample symbolizes the formation of PbI_2.

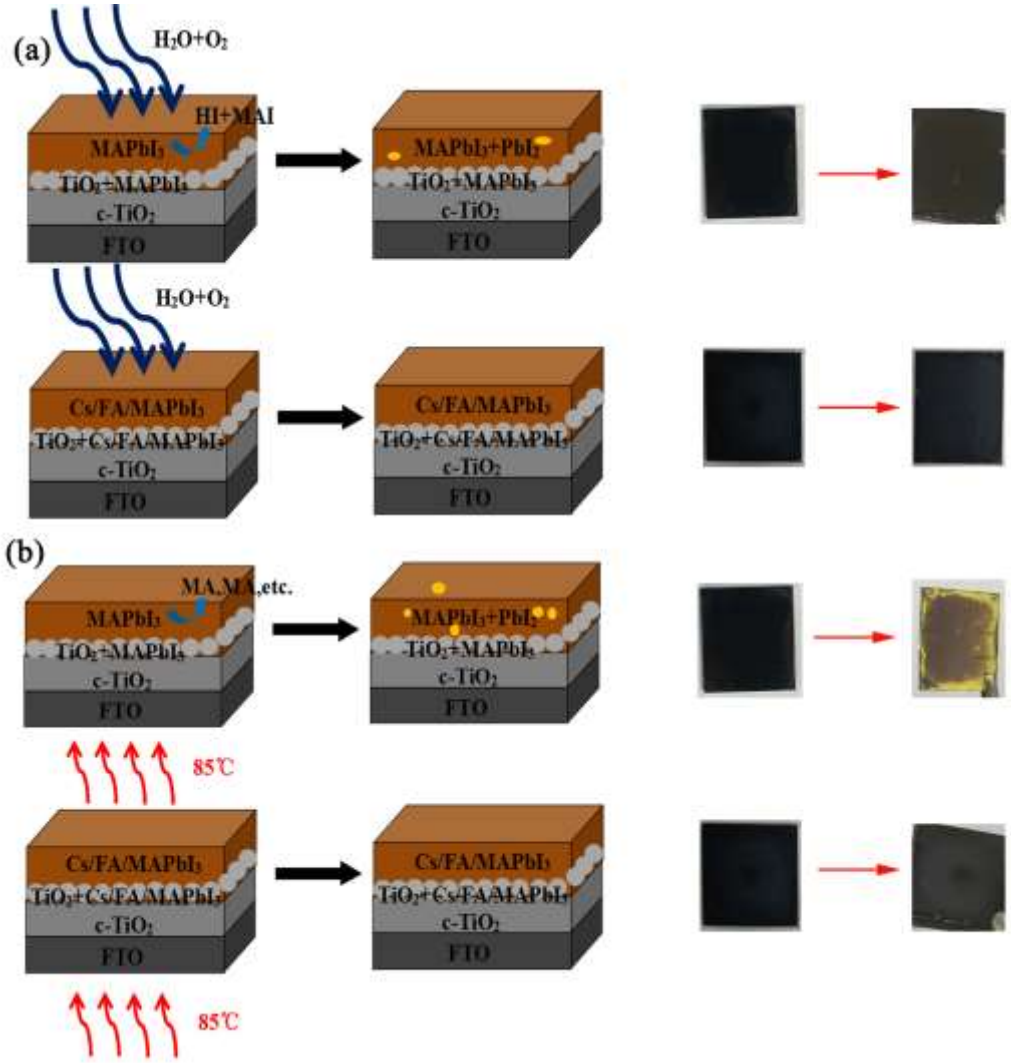

Fig. 6. (a) XRD spectra of the two kinds of perovskite film treated in an ambient environment (humidity 25%-35%, T = 25 °C) after 4 days and (b) annealed at 130 °C for 3 hours in dry air. (c) UV-visible absorption spectra of MA cation perovskite film and (d) triple cation perovskite film treated in an ambient environment (humidity 25%-35%, T = 25 °C) for 20 days. (e) UV-visible absorption spectra of MA cation perovskite film and (f) triple cation perovskite film annealed at 130 °C for 300 min in dry air.

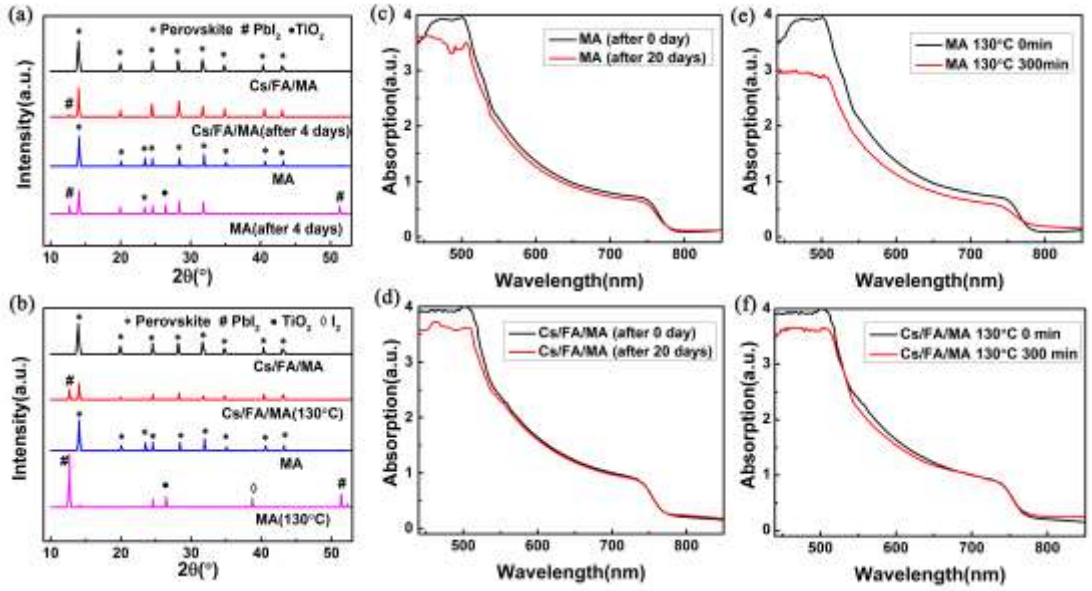

Table 1 Summary of the comparison between my work and that of others, showing the improved method, maximum PCE and stability.

	Perovskite film	Maximum PCE	Stability
Our work	Cs/FA/MAPb(I/Br)$_3$	18.2%	PCE was retained 88% after being treated in an ambient environment for 15 days
Choi and co-workers [27]	Cs/MAPbI$_3$	7.68%	PCE was retained 10% after 40 hours under ambient conditions
Park and co-workers [28]	Cs/FAPbI$_3$	19.0%	PCE was retained 20% after 60 min under continuous white light illumination in ambient condition
Snaith and co-workers [29]	MAPbI$_{3-x}$Cl$_x$+CsBr	16.3%	PCE was retained about 50% after 50 min upon UV irradiation
Qidong Tai and co-workers [30]	MAPbI$_{3-x}$(SCN)$_x$	15.12%	PCE was retained 86.7% after being stored in open air with the average RH level above 70% for over 500 h.

Table 2 Summary of results from J–V characteristics of devices included in the study, showing average values and the standard deviation (with best device data in parenthesis).

	V_{OC}(V)	J_{SC}(mA/cm^2)	FF(%)	PCE(%)
Cs/FA/MA	1.09±0.03(1.14)	22.98±0.2(23.3)	67.1±1.5(69.78)	16.84±0.5(18.2)
MA	1.01±0.03(1.04)	21.5±0.8(23.18)	64.4±2.1(68)	14.0±0.8(16.2)

Table 3 The parameters in the μ(t) function and σ(t) function.

	A	α(/h)	y_0	B(/h)
Cs/FA/MA (at 25 °C)	0.19	4×10^{-3}	0.8097	2.47×10^{-4}
MA (at 25 °C)	0.48	3×10^{-3}	0.53	2.33×10^{-4}
Cs/FA/MA (RH=60~80 %)	0.1928	5.68×10^{-3}	0.8072	2.42×10^{-4}
MA (RH=60~80 %)	0.54	4.36×10^{-3}	0.47	3.46×10^{-4}
Cs/FA/MA (at 85 °C)	0.2197	1.075×10^{-2}	0.7836	3.348×10^{-4}
MA (at 85 °C)	0.973	6.875×10^{-3}	2.691×10^{-2}	6.026×10^{-4}

Table 4 Estimated MTTF at room temperature when the relative humidity is 25 ~ 35%.

	P_{limit}	η(h)	β	MTTF(h)
Cs/FA/MA	$0.7P_0$	3974	0.82	4425.8
	$0.8P_0$	1518	0.81	1704.9
	$0.9P_0$	313.7	1.23	293.3
MA	$0.7P_0$	511	0.98	516
	$0.8P_0$	248.2	1.12	238.1
	$0.9P_0$	99.48	1.2	93.6

Table 5 Estimated MTTF at room temperature when the relative humidity is 60 ~ 80%.

	P_{limit}	η(h)	β	MTTF(h)
Cs/FA/MA	$0.7P_0$	3383	0.89	3581
	$0.8P_0$	1301	0.92	1353
	$0.9P_0$	218	1.09	211
MA	$0.7P_0$	339.7	1.07	330.9
	$0.8P_0$	137.7	1.22	129.0
	$0.9P_0$	59.6	1.37	54.5

Table 6 Estimated MTTF at 85 °C.

	P_{limit}	η(min)	β	MTTF(min)
Cs/FA/MA	$0.7P_0$	1671	0.9839	1682.7
	$0.8P_0$	479	0.99	479.7
	$0.9P_0$	76.9	1.30	71
MA	$0.7P_0$	62.51	1.338	57.4
	$0.8P_0$	39.19	1.35	35.94
	$0.9P_0$	17.43	1.45	15.80